IOPscience iopscience.iop.org

Home Search Collections Journals About Contact us My IOPscience

Formation of rhombic and superlattice patterns in bistable systems

This article has been downloaded from IOPscience. Please scroll down to see the full text article.

2001 Europhys. Lett. 54 612

(http://iopscience.iop.org/0295-5075/54/5/612)

View the table of contents for this issue, or go to the journal homepage for more

Download details:
IP Address: 132.236.27.111
The article was downloaded on 01/05/2012 at 01:38

Please note that terms and conditions apply.

EUROPHYSICS LETTERS 1 June 2001

Europhys. Lett., **54** (5), pp. 612–618 (2001)

Formation of rhombic and superlattice patterns in bistable systems

M. Bachir, S. Métens(*), P. Borckmans and G. Dewel

Service de Chimie-Physique and Center for Nonlinear Phenomena and Complex Systems - C.P. 231, Université Libre de Bruxelles, 1050 Bruxelles, Belgium

(received 29 September 2000; accepted in final form 26 March 2001)

PACS. 47.54.+r – Pattern selection; pattern formation.
PACS. 82.40.Bj – Oscillations, chaos, and bifurcations.

Abstract. – We investigate the selection of structures generated by diffusive instabilities in asymmetric bistable systems. It is shown that the nonlinear coupling between the zero mode and the different spatial modes emanating from the two homogeneous states can give rise to self-parametric instabilities favoring the occurrence of stable resonant rhombic and superlattice patterns.

Diffusive instabilities have proved to be a major pattern-forming mechanism in physics, chemistry, and materials science [1]. Many experiments and numerical works have studied the formation of such structures in systems that further exhibit the phenomenon of bistability between homogeneous steady states (HSS) [2–8]. On the other hand, most theoretical results in this field have been obtained in systems possessing a single HSS. There, in the case of supercritical or slightly subcritical bifurcations, a weakly nonlinear theory has been developed to tackle the pattern selection problem [9, 10]. The situation is more complicated in bistable systems where diffusion-driven instabilities can appear on both HSS. These instabilities in general interfere with the saddle-node bifurcations corresponding to the limit points of the bistability domain. We have indeed shown previously that large-amplitude structures can arise from the coupling between the spatial critical modes and the homogeneous mode that becomes marginal at the hysteresis limits [5, 11]. In that work, however, we have only considered symmetric bistable systems for which the hysteresis loop presents in phase space an inversion symmetry with respect to the critical point. The branches of patterned solutions issued from the two Turing instabilities then interconnect [5]. However, most experimental systems do not exhibit this nongeneric property. In this letter, we investigate the effects of the asymmetry of the hysteresis loop on the pattern selection problem. In the case at hand the critical wave numbers q_c^u and q_c^l associated with the two diffusive instabilities on the HSS are different. We show that the interaction between these spatial modes can give rise, through the coupling with the zero mode, to new self-resonance effects leading, for instance, to the stabilization of nonequilateral triangles which have been observed in boundary-fed reactors [12,13]. Similarly,

(*) Present address: Laboratoire de Physique Théorique de la Matière Condensée (Tour 24/14), Université de Paris 7 - 2 place Jussieu, 75251 Parix cedex 05 France.

© EDP Sciences

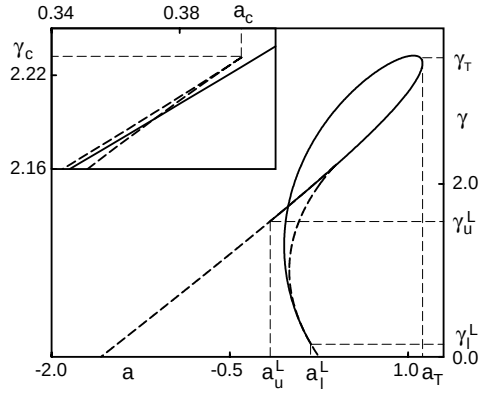

Fig. 1 – Schematic phase space $[a, \gamma]$ of the asymmetric FitzHugh-Nagumo model (eqs. (1), (2)) for $\beta = 0.99$, $d = 7.5$, and $\epsilon = 1.5$. Dashed and solid lines, respectively, denote the loci of the homogeneous saddle node bifurcations originating from the cusp at γ_c and of the Turing instabilities given by (γ_u^L γ_T γ_l^L).

we predict in such systems the onset of superlattice patterns [14] composed of two different but interacting sublattices, respectively, with wave numbers q_c^u and q_c^l.

For the sake of concreteness, we consider the following variant of the FitzHugh-Nagumo model (FHN):

$$\partial_t u = u - u^3 + \beta uv - v + \nabla^2 u, \tag{1}$$

$$\partial_t v = \epsilon(\gamma u - v - a) + d\nabla^2 v. \tag{2}$$

However, the results presented below have a wider range of application. Here $d = D_v/D_u$ and $\epsilon = T_u/T_v$ are, respectively, the ratio of the diffusion coefficients and characteristic chemical relaxation times of the activator u and inhibitor v. The parameters a, $\gamma(> 0)$ and $\beta(> 0)$ control the relative position and thus the number of intersections of the nullclines. In the following, we consider only cases where ϵ is such that a Hopf bifurcation never comes into play in agreement with the experimental situations we want to describe.

As the control parameter a is varied, bistability arises for $\gamma < \gamma_c$ through two back-to-back saddle node bifurcations at $a = a_u$ and $a = a_l$, linked by their unstable manifold and creating a hysteresis loop between two HSS inside the cusp region shown in fig. 1. When $\beta = 0$, the bistability domain is symmetric with respect to the critical point ($a_c = 0$, $\gamma_c = 1$). An increase of the parameter β induces a distortion of this symmetric hysteresis loop in the [u (or v), a]-plane.

In the presence of a differential diffusion process ($d > 1$), these HSS can be destabilized by inhomogeneous perturbations. In general, two Turing instabilities are created at (a_T, γ_T). In the [a, γ]-plane, when γ is decreased below γ_T, they migrate, invade the cusp region and approach the limit points. The location of the Turing thresholds respectively on the upper and lower branch is denoted a_u^T and a_l^T. For a given value of γ, the diffusive instability comes closest to the saddle node bifurcation whose curvature K_i ($i = u, l$) is the largest and the corresponding wave number is the smallest. In our model, we have $K_u > K_l$, and thus $q_u^c < q_l^c$; the Turing bifurcation on the upper branch is also the first to come in coincidence with the limit point a_u at $\gamma = \gamma_u^L$. For $\gamma < \gamma_u^L$, the pattern-forming instability only appears on the lower branch and when $\gamma < \gamma_l^L$, no more diffusive instability occurs on the HSS. The

results of this linear stability analysis which are common to many bistable systems [4,6–8] are summarized in fig. 1.

In previous works, we have shown that the homogeneous mode must be taken into account in order to obtain a global description of the development of the structures that can appear in bistable systems [5, 11]. We therefore approximate the concentration fields by a linear superposition of this homogeneous mode A_0, m_j critical modes associated with the diffusive instability on the lower branch ($\{A_j\}$) and m_k critical modes corresponding to the instability occurring at $a_{\mathrm{u}}^{\mathrm{T}}$ ($\{B_k\}$):

$$\boldsymbol{c} = \boldsymbol{e}_1 A_0 + \boldsymbol{e}_2 \sum_j A_j \exp\left[i\boldsymbol{q}_j^{\mathrm{l}} \cdot \boldsymbol{r}\right] + \boldsymbol{e}_3 \sum_k B_k \exp\left[i\boldsymbol{q}_{\mathrm{k}}^{\mathrm{u}} \cdot \boldsymbol{r}\right] + \text{c.c.}, \tag{3}$$

where $\boldsymbol{c} = \binom{u}{v}$ and $|\boldsymbol{q}_j| = q_{\mathrm{c}}^{\mathrm{l}}$; $|\boldsymbol{q}_k| = q_{\mathrm{c}}^{\mathrm{u}}$. The coefficients $\boldsymbol{e}_m$ are the eigenvectors of the corresponding Jacobian matrix. When $q_{\mathrm{c}}^{\mathrm{u}} \neq q_{\mathrm{c}}^{\mathrm{l}}$, this model exhibits standard patterns of smectic (stripes) and hexagonal symmetry of wave numbers $q_{\mathrm{c}}^{\mathrm{u}}$ or $q_{\mathrm{c}}^{\mathrm{l}}$ that emanate, respectively, from the instabilities at $a_{\mathrm{u}}^{\mathrm{T}}$ and $a_{\mathrm{l}}^{\mathrm{T}}$.

Moreover, the resonant interaction between the critical modes associated to these two Turing instabilities can give rise to stable rhombic patterns characterized by wave vectors forming isosceles triangles. One can distinguish two types of such structures:

$$\text{i)} \quad \boldsymbol{c} = \boldsymbol{e}_1 A_0 + \boldsymbol{e}_2\left(A_1 e^{i\boldsymbol{q}_1^{\mathrm{l}}\cdot\boldsymbol{r}} + A_2 e^{i\boldsymbol{q}_2^{\mathrm{l}}\cdot\boldsymbol{r}}\right) + \boldsymbol{e}_3 B_3 e^{i\boldsymbol{q}_3^{\mathrm{u}}\cdot\boldsymbol{r}}, \quad \text{with } \boldsymbol{q}_1^{\mathrm{l}} + \boldsymbol{q}_2^{\mathrm{l}} + \boldsymbol{q}_3^{\mathrm{u}} = 0, \tag{4}$$

$$\text{ii)} \quad \boldsymbol{c} = \boldsymbol{e}_1 A_0 + \boldsymbol{e}_3\left(B_1 e^{i\boldsymbol{q}_1^{\mathrm{u}}\cdot\boldsymbol{r}} + B_2 e^{i\boldsymbol{q}_2^{\mathrm{u}}\cdot\boldsymbol{r}}\right) + \boldsymbol{e}_2 A_3 e^{i\boldsymbol{q}_3^{\mathrm{l}}\cdot\boldsymbol{r}}, \quad \text{with } \boldsymbol{q}_1^{\mathrm{u}} + \boldsymbol{q}_2^{\mathrm{u}} + \boldsymbol{q}_3^{\mathrm{l}} = 0. \tag{5}$$

The corresponding amplitude equations can be written in the following compact form (case i)):

$$\frac{\mathrm{d}A_1}{\mathrm{d}t} = \mu_1(A_0)A_1 + \left(\nu - g_{ND}A_0\right)A_2^* B_3^* - g_D|A_1|^2 A_1 - g_{ND}\left[|A_2|^2 + |B_3|^2\right]A_1. \tag{6}$$

The equation for A_2 can easily be obtained from eq. (6) by permutation of indices 1 and 2,

$$\frac{\mathrm{d}B_3}{\mathrm{d}t} = \mu_2(A_0)B_3 + \left(\nu - g_{ND}A_0\right)A_1^* A_2^* - g_D|B_3|^2 B_3 - g_{ND}\left[|A_2|^2 + |A_1|^2\right]B_3, \tag{7}$$

$$\frac{\mathrm{d}A_0}{\mathrm{d}t} = f(A_0) + \left(\nu - g_{ND}A_0\right)\left[|A_1|^2 + |A_2|^2 + |B_3|^2\right] - g_{ND}\left[A_1 A_2 B_3 + A_1^* A_2^* B_3^*\right], \tag{8}$$

where $f(A_0) = 0$ determines the HSS. The linear growth rates $\mu_i(A_0)$, which are nonlinear functions of A_0, and the coupling constants can be expressed in terms of the parameters of the model. Similar equations can be derived in the case ii) by permuting the amplitudes A and B. These resonant patterns should not be confused with the unstable rhombic planforms characterized by two critical wave numbers of length q_{c}^i ($i =$ u or l) and making an angle such that their sum does not correspond to an active mode [10]. In the latter case, the phases of the modes are arbitrary. In contrast, from eqs. (6)–(8), it is easy to derive the following equation for the sum Φ of the phases of the modes:

$$\frac{\mathrm{d}\Phi}{\mathrm{d}t} = -\left(\nu - g_{ND}A_0\right)\left[\frac{S^2 + R^2}{S}\right]\sin(\Phi), \tag{9}$$

where $\Phi = \phi_1 + \phi_2 + \phi_3$, if $A_i = Re^{i\phi_i}$ ($i = 1, 2$) and $B_3 = Se^{i\phi_3}$. According to the sign of $(\nu - g_{ND}A_0)$, Φ relaxes to 0 or π leading to two types of conjugated structures. As in the case of regular hexagons, the sum of the phases of the modes forming the isosceles triangles

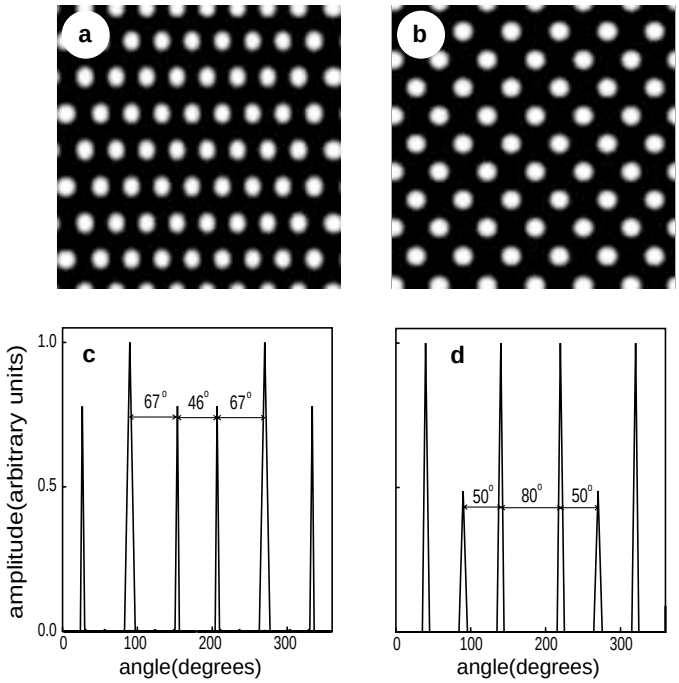

Fig. 2 – 2D rhombic patterns obtained by numerical integration of the FitzHugh-Nagumo model (eqs. (1), (2)) at $a = -0.1$, $\beta = 0.7$, $\gamma = 0.9$, $\epsilon = 2.5$, and $d = 120$. (a) and (b): Rhombs corresponding, respectively, to cases i) and ii) for which the sum of the phases of the modes $\Phi = 0$. (c) and (d): Angular amplitude distribution in spatial frequency space for the patterns in (a) and (b), respectively.

adjusts in such a way as to favor the occurrence of these resonant rhombs. In fact, they can be obtained by stretching a hexagonal array along one of its symmetry axes. As a consequence, the corresponding Fourier transform presents either two large and four small peaks (case i)) or four large and two small amplitudes (case ii)) (figs. 2(c) and (d)). These rhombs can coexist with the regular hexagonal patterns in the vicinity of the instability points (cf. fig 3).

Such rhombs have been obtained in experiments on the chlorite-iodide-malonic acid reaction (CIMA) [12,13]. The CIMA reaction is known to exhibit a variety of nonlinear behaviors such as oscillations, bistability [15] and Turing structures [16,17]. The reaction takes place in a thin gel disk reactor which is sandwiched between two continuously fed well-stirred tanks in which the concentrations are maintained constant. The components of the reaction are distributed in the two reservoirs in such a way that neither compartment is separately reactive. In such boundary-fed reactors, gradients of concentration develop inside the gel and the control parameter a thus presents a spatial variation in a direction perpendicular to the feeding planes leading to the unfolding in space of the corresponding bifurcation diagram. Two Turing instabilities then determine a spatial stratum of width Δ wherein the HSS is linearly unstable. When $\Delta \leq q_{\mathrm{c}}^{-1}$ quasi–two-dimensional resonant structures can develop in the transverse direction.

In order to explain the occurrence of these nonequilateral triangles, Gunaratne *et al.* [12,13] considered a system that exhibits a single Turing instability. Above the threshold, there exist in each direction of the Fourier spectrum a whole band of unstable modes. So it is possible

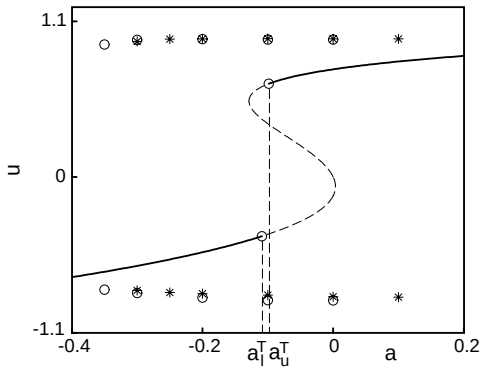

Fig. 3 – Bifurcation diagram limited (for simplicity) to rhombs ($\circ$) and the hexagons ($*$) emanating from the bifurcation point at a_l^T, obtained by numerical integration of the FHN model (eqs. (1), (2)) with $\beta = 0.7$, $\gamma = 0.9$, $\epsilon = 2.5$, and $d = 120$.

to construct solutions characterized by wave vectors of different lengths and lying inside the instability region. Numerical integrations of a modified Landau-Ginzburg equation then produce stable rhombic patterns. The modifications include the use of the so-called Gunaratne operator: $\Box_j = \boldsymbol{n}_j \cdot \nabla - (i/2q_c)\nabla^2$ (with $\boldsymbol{n}_j = \boldsymbol{k}_j/k_c$) to describe the spatial modulations of the amplitudes and also the addition of new nonlinear terms which do not however play an essential role in the stabilization of these patterns. Since they violate the conditions that require all terms in the amplitude equations to be the same order of magnitude, these modifications have been the object of severe criticisms by several authors [18–20]. In this paper, we present a simple mechanism that explains why nonequilateral triangles corresponding to hexagons deformed along one of their axes can be formed in these two-side–fed reactors [21]. Clearly figs. 2(a) and (b) correspond, respectively, to figs. 6d and 6c obtained in experiments on CIMA reaction [21]. Numerical studies in large systems also exhibit the spatial coexistence of regular and distorted hexagons as in the experiments. Various observations indeed indicate that in these experiments the system is not too far from a cusp point. For instance, a variation of malonic acid concentration can induce a transition *via* the unstable uniform state, between two hexagonal patterns differing only in their wavelengths [21]. Also, the sequence: hexagons/stripes/re-entrant hexagons with a different wavelength has been generated by a change of the control parameter [21]. These results and others are consistent with the theory presented above. This explanation allows also to understand why such structures have not been observed in standard pattern-forming instabilities (Rayleigh-Bénard).

When the critical wave numbers are sufficiently different, superlattice structures can also be easily generated. As shown in fig. 4(b), they correspond to patterns that have structures on the two length scales $2\pi/q_c^u$ and $2\pi/q_c^l$ dictated by the instabilities appearing on the HSS. In Fourier space, they are characterized by wave vectors forming resonant triplets (equilateral triangles of lengths q_c^u or q_c^u and the isosceles triangles defined above). An example is shown in fig. 4(a) of a superlattice with 9 modes. The corresponding planform then takes the following form:

$$\boldsymbol{c} = \boldsymbol{e}_1 A_0 + \boldsymbol{e}_2 \sum_{j=1}^{3} A_j \exp\left[i\boldsymbol{q}_j^l \cdot \boldsymbol{r}\right] + \boldsymbol{e}_3 \sum_{k=1}^{6} B_k \exp\left[i\boldsymbol{q}_k^u \cdot \boldsymbol{r}\right] + \text{c.c.}, \tag{10}$$

with $\boldsymbol{q}_1^l + \boldsymbol{q}_2^l + \boldsymbol{q}_3^l = 0$, $\boldsymbol{q}_1^l + \boldsymbol{q}_1^u + \boldsymbol{q}_2^u = 0$, $\boldsymbol{q}_2^l + \boldsymbol{q}_3^u + \boldsymbol{q}_4^u = 0$, and $\boldsymbol{q}_3^l + \boldsymbol{q}_5^u + \boldsymbol{q}_6^u = 0$.

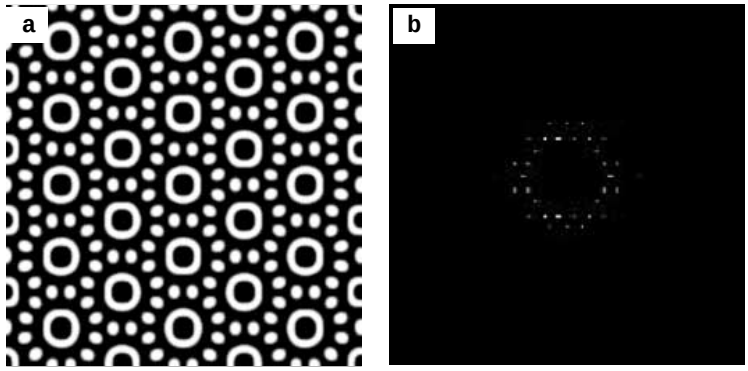

Fig. 4 – (a) Superlattice Turing pattern (cf. eq. (10)) obtained from a numerical integration of the FHN model (eqs. (1), (2)) for $\beta = 0.7$, $\gamma = 0.9$, $\epsilon = 2.5$, and $d = 120$. (b) The corresponding Fourier transform showing two critical circles of length q_c^l and q_c^u, respectively.

As preceedingly, coupled amplitude equations can be derived. Here also, it is the sign of the quadratic term that determines the sum of the phases in each resonant triad. Dynamic superlattice structures have been obtained in nonlinear optical devices [22, 23] and in two-frequencies Faraday experiments [24, 25]. More recently, the stability of stationary superlattices generated by a single Turing instability on a regular lattice has also been studied [20]. The corresponding wavelength is then chosen in such a way that the lattice can accommodate a pattern of given symmetry. On the other hand, in the bistable systems we have considered, the two wave numbers are naturally associated to the two Turing instabilities on the HSS. It is indeed well known [20, 26] that rhombic patterns or quasiperiodic structures cannot bifurcate from a Turing instability on a single HSS. In the absence of zero mode, the instability of these patterns is only guaranteed if the linearized eigenvalues associated to the two families of critical modes are all negative. This implies the existence of a bistability domain and the homogeneous mode A_0 must then be incorporated in the dynamical description. As a result, our scenario does not reduce to the models introduced preceedingly from a study of *ad hoc* reaction-diffusion systems [26, 27].

Finally, resonant interactions between the two families of critical modes also occur in the case of structures periodic in one direction (stripes) when the critical wave numbers satisfy the condition $q_c^l = 2q_c^u$. Only the patterns with the largest wave number q_c^l then survive. This provides a nice example of self-entrainment of spatial modes emanating from different branches of the bistable. It should not be confused with the $1 : 2$ resonance that occurs when the first superharmonic of the critical mode becomes active in a system exhibiting a pattern-forming instability with a flat dispersion curve [28]. In bistable systems, the coupling with the zero mode prevents the onset of the drift instability and reinforces the stability of the pattern with wave number $q_c^l = 2q_c^u$. A similar self-resonance effect again occurs when $q_c^l = 3q_c^u$; two types of patterns with wave numbers $2q_c^u$ and $3q_c^u$ are then obtained according to the initial conditions.

The mechanisms presented above are still operative in the monostable region but close to the critical point.

In conclusion, we have shown that asymmetric bistable systems present further examples of self-induced resonances resulting from the interaction between two different symmetry-breaking instabilities [23, 29]. Here it is the spatial modes associated to one of the diffusive

instabilities that play the role of the forcing of the other. As a result, these systems provide good candidates for the experimental observation of superlattice Turing patterns.

* * *

We thank L. PISMEN for interesting comments. This work was supported by Grants of the CGRI-FNRS/CNRS and the "Fondation Universitaire D. and A. VAN BUUREN" (Belgium). PB and GD received support from the FNRS (Belgium) and MB from the "Direction de l'Enseignement Supérieur" (Morocco).

REFERENCES

[1] WALGRAEF D., *Spatio-Temporal Pattern Formation* (Springer, Berlin) 1997.
[2] AFANAS'EV A. A. *et al.*, *Opt. Commun.*, **115** (1995) 559.
[3] BREAZEAL W., FLYNN K. M. and GWINN E. G., *Phys. Rev. E*, **52** (1995) 1503.
[4] ACKEMANN T. *et al.*, *Phys. Rev. Lett.*, **75** (1995) 3450.
[5] MÉTENS S. *et al.*, *Europhys. Lett.*, **37** (1997) 109.
[6] MICHAELIS D., PESCHEL U. and LEDERER F., *Phys. Rev. A*, **56** (1997) R3366.
[7] HORVÁTH D. and TÓTH Á., *J. Chem. Soc. Faraday Trans.*, **93** (1997) 4301.
[8] HILDEBRAND M., MIKHAILOV A. S. and ERTL G., *Phys. Rev. E*, **58** (1998) 5483.
[9] CROSS M. C. and HOHENBERG P. C., *Rev. Mod. Phys.*, **65** (1993) 854.
[10] MALOMED B. A. *et al.*, *Physica D*, **70** (1994) 357.
[11] DEWEL G. *et al.*, *Phys. Rev. Lett.*, **74** (1995) 4647.
[12] OUYANG Q., GUNARATNE G. H. and SWINNEY H. L., *Chaos*, **3** (1993) 707.
[13] GUNARATNE G. H., OUYANG Q. and SWINNEY H. L., *Phys. Rev. E*, **50** (1994) 2802.
[14] SILBER M., PROCTOR M. R. E., *Phys. Rev. Lett.*, **81** (1998) 2450.
[15] DE KEPPER P., BOISSONADE J. and EPSTEIN I. R., *J. Phys. Chem.*, **94** (1990) 6255.
[16] CASTETS V. *et al.*, *Phys. Rev. Lett.*, **64** (1990) 2953.
[17] OUYANG Q. and SWINNEY H. L., *Nature*, **352** (1991) 610.
[18] NEPOMNYASHCHY A. A. and PISMEN L. M., *Phys. Rev. Lett.*, **72** (1994) 944.
[19] PISMEN L. M. and NEPOMNYASHCHY A. A., *Europhys. Lett.*, **24** (1993) 461.
[20] JUDD S. L. and SILBER M., *Physica D*, **136** (2000) 45.
[21] OUYANG Q. and SWINNEY H. L., in *Chemical Waves and Patterns*, edited by R. KAPRAL and K. SHOWALTER (Kluwer, Dordrecht) 1995, pp. 269-295.
[22] PAMPALONI E. *et al.*, *Phys. Rev. Lett.*, **78** (1997) 1042.
[23] MUSSLIMANI Z. H. and PISMEN L. M., *Phys. Rev. E*, **62** (2000) 389.
[24] KUDROLLI A., PIER B. and GOLLUB J. P., *Physica D*, **123** (1998) 99.
[25] ARBELL H. and FINEBERG J., *Phys. Rev. Lett.*, **81** (1998) 4384.
[26] FRISH T. and SONNINO G., *Phys. Rev. E*, **51** (1995) 1169.
[27] LIFSHITZ R. and PETRICH D. M., *Phys. Rev. Lett.*, **79** (1997) 1261.
[28] PROCTOR M. R. E. and JONES C. A., *J. Fluid Mech.*, **188** (1988) 301.
[29] DE WIT A. *et al.*, *Phys. Rev. E*, **54** (1996) 261.